# SATELLITES, OCEANOGRAPHY AND SOCIETY

Edited by

**David Halpern** 

Jet Propulsion Laboratory, California Institute of Technology, Pasadena, USA



2000 ELSEVIER

Amsterdam – Lausanne – New York – Oxford – Shannon – Singapore – Tokyo

# Chapter 2

# Development and application of satellite retrievals of ocean wave spectra

Patrick Heimbach and Klaus Hasselmann Max-Planck-Institut für Meteorologie, Hamburg, Germany

Abstract. The launch of SeaSat in 1978 demonstrated the feasibility of measuring ocean wave heights and imaging the corresponding two-dimensional wave field from space. With the launch of the first European Remote-sensing Satellite (ERS-1) in 1991, wave researchers and operational forecasters obtained global, continuous, quasi-real-time wave data for the first time. This led to the developments of sophisticated, so-called "third-generation" wave models, such as the Wave Model (WAM), and spectral retrieval algorithms for synthetic aperture radar (SAR) data. To achieve these goals, however, significant hurdles had to be overcome. Wave modelers had to develop numerically viable parameterizations of the nonlinear wave-wave interactions. The remote-sensing challenge was to understand and resolve the strong nonlinearities besetting SAR imaging of the moving ocean wave surface. This paper reviews the progress achieved over the last twenty years and summarizes wave data assimilation methods and other current applications of ERS quasi-real-time global SAR wave spectral data or SAR wave-mode product.

Two applications are presented. A comparison of wave spectra predicted by WAM with spectra retrieved from ERS-1 on a global scale revealed that WAM overpredicted local wind-generated sea surface heights and underpredicted swell. The former can be largely attributed to wind-forcing errors, while the latter is most likely due to an overly strong swell dissipation in WAM. Assimilation of ERS-1 altimeter sea surface height data into the WAM spectra was found to not alter the qualitative conclusions of the comparison. A second application addresses the trans-ocean propagation of swell. Swell propagating from a storm in the South Pacific is traced over a period of ten days with ERS-1 SAR and compared with model predictions. Wind fields used for wave predictions are also compared with ERS-1 wind scatterometer data.

#### 1. Introduction

Major increases in computing performance have enabled the development of comprehensive atmospheric and oceanic general circulation models (A/OGCMs). A similarly

impressive expansion of global datasets available for initialization, validation, and assimilation into A/OGCMs has been enabled by a series of sophisticated Earth-observing satellite missions. Although less well known, similar efforts have been undertaken in the field of ocean wave remote sensing and modeling.

Since surface wave fields are two dimensional, a statistical description of local sea state requires the two-dimensional spectrum,  $F(\mathbf{k})$ , of the distribution of wave energy (or, equivalently, the variance of sea surface elevation) with respect to the propagation wavenumber,  $\mathbf{k}$ . Modern, state-of-the-art third-generation wave models, such as the Wave Model (WAM) (WAMDI Group 1988), solve a spectral energy balance equation for the evolution of  $F(\mathbf{k})$  under the influence of wave generation by wind, nonlinear wave-wave interactions, and dissipation due to wave breaking. For a detailed overview, see Komen et al. (1994). WAM is currently operational at numerous numerical weather prediction (NWP) centers, such as the European Centre for Medium-Range Weather Forecasts (ECMWF), and is implemented at about 120 research institutions worldwide. A recent evaluation of four widely used contemporary wave models may be found in Cardone et al. (1996) in relation to two rare extreme events in the North Atlantic: the "Storm of the Century" of March 1993 and the "Halloween Storm" of October 1991, an account of which was given in the best-seller by Junger (1997).

Various techniques have been developed to assimilate satellite and in-situ wave measurements into wave models. Janssen and Viterbo (1996) have shown the important role of the moving sea surface in the transfer of momentum and, presumably, other properties across the air-sea interface. As a consequence, NWP centers have started (e.g., ECMWF) or others are planning (e.g., United Kingdom Meteorological Office, Deutsches Wetterdieust) to couple wave models to their operational atmospheric GCMs to provide a more realistic boundary condition at the air-sea interface.

The ocean-observing satellites ERS-1/2 and the follow-on Environmental Satellite (ENVISAT) motivated the development of more-sophisticated wave models than the operational models of the 1980s. Limitations of these parametric models were compiled by the SWAMP Group (1985). The ERS-1/2 missions have been able, for the first time, to provide continuous, global, near-real-time measurements of both significant wave height and the two-dimensional wave spectrum. Other satellites, such as the geodetic satellite (Geosat) and the Topography Experiment (TOPEX)/Poseidon satellite, which carry radar altimeters, have also provided accurate measurements of significant wave height, but only in an off-line mode. While these data were valuable for model validation and wave statistics, the near-real-time ERS radar altimeter wave height data, in combination with real-time measurements of the two-dimensional wave spectrum with a synthetic aperture radar (SAR) operating in a global mode, offered an exciting new prospect for operational wave forecasting and research. However, this is only possible with retrieval algorithms and wave models that fully exploit the two-dimensional wave spectral information contained in the SAR data. The focus of this review, therefore, is on methods of

retrieval of two-dimensional wave spectra from SAR image spectra and application of the retrieved wave spectra. Satellite missions carrying radar sensors applicable to ocean wind and wave measurements are summarized in Table 1.

The SAR is an all-weather, day-and-night, side-looking radar that emits short microwave pulses and processes a two-dimensional image from the received backscatter electromagnetic radiation. The cross-track, or range, coordinate of the backscattered energy is inferred, as is the case with a real-aperture radar (RAR), from the travel time of the pulse from emission to reception. The along-track, or azimuth, coordinate is reconstructed from the Doppler phase history of the signal produced by the moving platform. Unfortunately, satellite SAR ocean wave imaging is usually strongly nonlinear from the motions of the backscattering wave field, which create spurious Doppler shifts in the backscattered signal and produce misplacements of the backscattering surface elements in the image plane. For a long time, the resulting image distortion and associated partial loss of information at high azimuthal wavenumbers deterred researchers from using SAR data for quantitative ocean wave studies. Thus, at the time of the launch of the first oceanographic satellite, SeaSat, in 1978, ocean wave imaging by a SAR was still being evaluated, with many open questions. Today, however, a clearer understanding of how the wave spectrum is mapped into the SAR image spectrum, leading to the derivation of a closed, nonlinear, spectral mapping relation and the development of operationally viable retrieval algorithms, together with extensive validations of satellite spectral retrievals, have clearly established the usefulness of the SAR as a quantitative wave spectral measurement system.

#### 1.1 SeaSat

Despite having a lifetime of only three months in 1978, SeaSat clearly demonstrated that a spaceborne radar altimeter was capable of quantitatively measuring significant wave heights and that the two-dimensional ocean wave pattern could be successfully imaged with a SAR. However, analysis of SAR data also clearly demonstrated that the linear modulation transfer function relating the SAR image spectrum to ocean wave spectrum, which had been used for the airborne SAR, was in general not applicable for a spaceborne SAR. For a high-flying platform (i.e., one crossing the sky with a low angular velocity relative to a ground observer), the nonlinearity of the imaging mechanism can no longer be regarded as weak (Alpers et al. 1981). In principle, this problem could have been solved by deriving two-dimensional spectra in near-real-time from the SAR signal, without the intermediate step of first forming an image (Hasselmann 1980). This approach required excessive computer resources because of the inapplicability of fast Fourier transform (FFT) algorithms. The high volume of SAR data also precluded storing SAR data on board the satellite. As a result, the data had to be transmitted in real time to a small number of line-of-sight ground stations. Although current spaceborne SAR missions provide onboard data recorders, data storage facilities for full-swath SAR images are still limited

 $\Diamond = manned mission$ , \* = planned launch, • = planned end date). Table 1. A list of satellite missions for studies of ocean surface waves (Scat = scatterometer, SAR= synthetic aperture radar,

ALOS Japan	RADARSAT-II Canada	METOP-1 EUMETSAT	ALMAZ-1B Russia	ADEOS-2 USA/JF	JASON-1 USA/F	ENVISAT-1 ESA	LACROSSE USA	OKEAN-O Russia	QUIKSCAT USA	GFO USA		R <sub>o</sub>	RADARSAT-1 Canada		SIR-C <sup>◊</sup> USA		TOPEX/Poseidon USA/F	JERS Japan	ERS-1 ESA	ALMAZ-1 Russia	GEOSAT USA	OS-1870 I		SIR-A <sup>♦</sup> USA	SEASAT USA		SKYLAB <sup>◊</sup> USA	Satellite Country
n 2002*	da 2002*	SAT 2001*	ia 2001*	JP 2000*	/F 2000*	2000*			19/6/1999	10/2/1998	JP 4/8/1996	ia 23/04/96	da 4/11/1995	21/4/1995	30/9/1994	9/4/1994	F 10/8/1992	n 11/2/1992	16/7/1991	a 31/3/1991	12/5/1985	a 7/1987	05/10/1984	12/11/1981	27/6/1978	14/4/1975	25/5/1973	ry From
2005	2005	2004	2004	2004	2004	2004	multi-satellite series	multi-satellite series	2001	2002	30/6/1997	2000	2000	2000	11/10/1994	20/4/1994	2000	1999	02/06/1996	17/10/1992	1/1990	10/1989	13/10/1984	14/11/1981	9/10/1978	1/12/1978	8/2/1974	Until
-	1	I	yes	Ĩ	yes	yes	1	1	1	yes	1	yes	1	yes	1	1	yes		yes	1	yes	1	İ	1	yes	yes	yes	Altimeter
l	I	AScat	yes	SeaWinds	1				SeaWinds		NSCAT	Î		yes	Ī	Ĭ	1	I	yes	1		I	Ì	Í	yes	1	1	Scat
PALSAR	yes		yes	I	Ĩ	ASAR	yes	yes	1		]	yes	yes	yes	yes	yes	1	yes	yes	yes	1	yes	yes	yes	yes		1	SAR
yyy.tksc.nasda.go.jp/Home/Eartn_Obs/e/alos_e.num	radarsat.space.gc.ca/info/future.html	earth.esa.int/METOP.html	www.neosoft.com/Almaz/almaz1b/	adeos2.hq.nasda.go.jp/default_e.htm	topex-www.jpl.nasa.gov/jason1/	envisat.estec.esa.nl	solar.rtd.utk.edu/~mwade/craft/lacrosse.htm	solar.rtd.utk.edu/~mwade/project/okean.htm	winds.jpl.nasa.gov/missions/quikscat/quikindex.html	gfo.bmpcoe.org/Gfo/	echo.gsfc.nasa.gov/adeos/adeos.html	www.ire.rss.ru/priroda/priroda.htm	radarsat.space.gc.ca/	earth.esa.int/ersnewhome	southport.jpl.nasa.gov/in7dex.html	southport.jpl.nasa.gov/index.html	topex-www.jpl.nasa.gov/	yyy.tksc.nasda.go.jp/Home/Earth_Obs/e/Jers_e.html	earth.esa.int/ersnewhome	www.neosoft.com/Almaz/			southport.jpl.nasa.gov/index.html	southport.jpl.nasa.gov/index.html	www.earth.nasa.gov/history/seasat/seasat.html			URL: http://

(e.g., 10 min per 100 min orbit for ERS-1/2, 28 min per 100 min orbit for RadarSat, 30 min per 100 min orbit planned for ENVISAT). In principle, the high data rate problem can be overcome by transmitting the data via relay satellites, but this is not expected to be available globally for SAR satellites in the near future. Nevertheless, limited data-relay capabilities will be provided for ENVISAT, which will be launched in 2000.

# 1.2 European Remote-sensing Satellite

The first European Remote-sensing Satellite (ERS-1) was launched in July 1991 from Kourou, French Guiana, into a near-polar, sun-synchronous orbit yielding coverage between 81.5°S and 81.5°N. After ERS-2 was launched in April 1995, both satellites were operated in tandem between August 1995 and May 1996. ERS-2 follows ERS-1 with an approximate 30-min time lag in the same orbital plane, so that there is a 1-day interval between ERS-1 and ERS-2 observing the same ground swath. While this simultaneous operation of two spaceborne SARs has enabled a variety of novel applications, particularly related to interferometry at time scales longer than one day, the impact for wave applications remained limited due to large temporal wind and wave variability. Nevertheless, the simultaneous operation enabled cross-calibration between both satellites' sensors. ERS-1 was switched into a dormant mode in June 1996. The launch of ENVISAT (Section 1.3) ensures continuity of SAR data into the next millennium.

With respect to surface wave measurements, the main advance of ERS relative to SeaSat is the implementation of near-real-time processing for both altimeter and SAR measurements, as well as global sampling for the SAR, enabling SAR wave mode data to be used for global studies and operational wave forecasting. Data storage limitations of the SAR are surmounted with a subframe image mode specifically designed for ocean wave measurements. This so-called SAR wave mode (SWM) is switched on every 200 km, producing a 5-km × 10-km SAR image (or "imagette"). The average data rate relative to the continuously operating standard SAR imaging mode, which has a swath width of 100 km, is reduced by a factor of 100. Imagettes in a global, locally intermittent mode are stored on board and transmitted to a ground station once per orbit. The imagettes are the amplitude averages of three successive looks and are Fourier transformed to wavenumber spectra, which are then bin-averaged to reduced 12 × 12 polar wavenumber spectra. These spectra are disseminated by the European Space Agency (ESA) as a fast delivery product (FDP) in quasi-real time to NWP centers. With the exception of occasional gaps, primarily near coasts and the ice edge, where the SAR is operated in the full-swath mode providing precision images, the SAR yields daily coverage of the global wave spectral field at an alongtrack resolution comparable with typical NWP models and a cross-track resolution, dependent on latitude, of 1000-2000 km, which is a lower resolution than NWP models.

The SWM is interlaced in the swath of the simultaneously operating wind scatterometer (WNS). The SWM footprint at 19.9° incident angle corresponds to the second of

19 scatterometer range nodes, from near range to far range, separated by 25 km. This enables simultaneous recording and analysis of both wind and wave data (e.g., Chapron et al. 1995; Kerbaol et al. 1998). This complements the ongoing efforts to apply ERS SAR imagery to high-resolution scatterometry (e.g., Vachon and Dobson 1996; Scoon et al. 1996; Lehner et al. 1998; Hφgda et al. 1998). The scatterometer is comprised of three antennas measuring normalized radar cross-section (NRCS) from which the mean surface wind speed and direction over a 50-km × 50-km area can be extracted. An atlas of global wind fields produced between 1991 and 1996 has been published by Bentamy et al. (1996). The scatterometer and SAR operate at the same C-band (5.6 cm) wavelength and are combined in a single active microwave instrument (AMI), enabling the development and mutual validation of the same microwave backscatter models for both sensors (Johannessen et al. 1998).

The radar altimeter provides a third simultaneous source of wind and significant wave height data. However, it operates at Ku-band (13.8 GHz), and its nadir position is separated by about 270 km from the SWM imagette location. Wind speed is extracted from the intensity of the return echo signal; wave height is extracted from the slope of the leading edge of the return echo signal.

## 1.3 Environmental Satellite

The launch of ENVISAT is scheduled for late 2000. ENVISAT will carry the Advanced SAR (ASAR) instrument, which will feature a number of enhanced capabilities. ASAR can operate in five mutually exclusive modes. During a global mission, which requires a low data rate for full operationality, ASAR is switched either into the global monitoring (ScanSAR) mode or into the wave (imagette) mode, comparable to ERS SWM. During a regional mission, which requires a high data rate, ASAR is operated either in image mode or alternating polarization mode (both are 30-m × 30-m resolution with 55- to 100-km swath), or the wide-swath mode (150-m × 150-m resolution with 405-km swath). Changing the incident angle between 15° and 45° allows one of seven possible subswaths to be selected. Images may also be taken at different polarizations.

A novel feature, important for wave monitoring, is the ability to overcome the directional ambiguity problem by exploiting information on time-dependent changes in the wave field. These changes are contained in successive single-look images, which normally are simply superimposed to produce a reduced-speckle multi-look image. Pairs of successive single-look images are generated from different subbands of the full-bandwidth Doppler spectrum. A cross-spectrum is computed from these pairs, which are typically separated in time by a fraction of the dominant wave period. The wave's dominant travel direction may be determined from the cross-spectrum.

Cross-spectrum analysis enables a second problem of SAR imagery to be efficiently tackled: the reduction of speckle noise. Speckle, which refers to the grainy appearance of SAR images, arises through coherent (phase-related) contributions of differential scatter-

ers within a resolution cell (pixel). In contrast, the point-spread functions of different pixels in the image are completely dephased. Speckle noise can be considered a random walk problem and, for Gaussian processes, reduces to a multiplicative noise contribution. Conventionally, speckle noise is reduced by means of multi-look averaging, where single-look images are added up incoherently, yielding a speckle-reduced image (e.g., Gower 1983; Vachon and West 1991; Johnsen 1992). This approach reduces the wave image contrast because the target is stationary. The cross-spectrum computed from single-look images completely removes the speckle contribution for white noise, while avoiding image contrast reduction caused by moving waves.

Ambiguity removal was first considered in the context of ship radars by Atanasov et al. (1985), Rosenthal et al. (1989), and Rosenthal and Ziemer (1991). Various studies have subsequently been performed with airborne SARs (e.g., Raney et al. 1989; Vachon and Raney 1991). The cross-spectrum was incorporated into a SAR-to-wave nonlinear spectral inversion algorithm, first for airborne SAR data (Engen and Johnsen 1995a), and then for ERS-1 SAR images (Engen and Johnsen 1995b). The cross-spectrum is planned to be part of the fast delivery wave mode product for ENVISAT (Johnsen and Desnos 1999).

## 1.4 Theory of synthetic aperture radar ocean wave imaging

At the time of SeaSat, there were numerous theories for the SAR imaging of ocean waves, but no consensus on the proper description of how to map a moving, random sea surface into a SAR image and the associated two-dimensional spectra. Among the main issues (e.g., Allan 1983; Ulaby et al. 1986) were questions relating to the applicability of the two-scale concept of moving point scatterers (facets), the relevance of Bragg scattering theory, the role of radar polarization, the form of linear modulation transfer functions, the relationship between scene coherence time and dynamics of scattering waves, the impact of speckle noise on signal-to-noise, calibration, image degradation due to orbital facet acceleration, the relative importance of the phase and orbital velocities of waves, and—most important of all—the quantitative description of nonlinear image distortions induced by wave motions. These nonlinearities frequently prevented the detection of ocean waves and made the interpretation of imaged waves difficult.

One of the more ambitious SAR aircraft campaigns, designed to resolve many contentious issues regarding SAR ocean wave imaging, was carried out during the Marine Remote Sensing (MARSEN) project in the summer of 1979 in the North Sea. MARSEN data reconciled different views on SAR imaging of a moving, random, ocean wave surface within the framework of a consistent, comprehensive theory (Hasselmann et al. 1985; Tucker 1985). Individual Bragg backscattering facets of large dimension compared with radar wavelength, but small compared with typical wavelengths of surface waves, are mapped individually into pixels (Wright 1968; Valenzuela 1978) in the image plane. The separability of the mapping mechanism on the facet scale is justified by the phase decorrelation, but not amplitude independence, of the separate facet return signals.

The motion of the scatterers of a facet induces a Doppler frequency in the return signal, which translates into an azimuthal displacement of the facet in the image plane. The effective velocity of the scatterers is given by the sum of the phase velocities of the backscattering wave perturbations propagating on the facets and the significantly larger eigenmotions of the facets due to the orbital motions of the long waves. To a first approximation, the scatterer velocity can be regarded as constant during the SAR illumination time, so that the Doppler spectrum of an individual facet is a single narrow line. However, the Doppler spectrum for an ensemble of facets with different effective scatterer velocities is a broad Gaussian distribution, and the corresponding distribution of the facet positions in the image plane is nonuniform. For small wave steepness, the modulation of the facet positions in the image plane by the long-wave orbital velocity ("velocity bunching") enhances the RAR imaging due to the direct modulation of the scattering cross-section by the long waves, but for higher wave steepness, the image is smeared in the azimuthal direction. For a quantitative analysis of these effects, the coherence time of the backscattered facet signals was found to be a less useful concept than the Doppler spectrum of the facet return signals, which can be expressed directly in terms of the kinematic and dynamical properties of the facet elements.

The velocity bunching mechanism has been extensively studied theoretically and verified by experiments (Alpers and Hasselmann 1978; Alpers and Rufenach 1979; Swift and Wilson 1979; Valenzuela 1980; Raney 1980; Plant and Keller 1983). The component,  $\upsilon$ , of the wave orbital motion in the direction of the satellite induces an additional Doppler shift that leads to an additional azimuthal displacement

$$\Delta x = \frac{R}{U}v$$

of the facet in the SAR image domain, where R is the slant range and U is the platform velocity. For small displacements,  $\Delta x$ , compared with the wavelength,  $\lambda$ , of the waves being imaged, the alternate bunching and spreading of the facet positions by the orbital wave motion enhances the imaging and can be described by a linear modulation transfer function, which can be added to the analogous RAR modulation transfer function. However, when the displacements become comparable to or larger than  $\lambda$ , the wave structure in the image plane becomes convoluted, and the mapping of the wave spectrum into the image spectrum is no longer linear. The nonlinear image degradation is governed by the ratio:

$$\frac{\Delta x}{\lambda} = \frac{\omega}{\omega_s} \frac{h}{\lambda}$$

where  $\omega$  and h denote the frequency and height of the waves, respectively, and:

$$\omega_s = \frac{U}{R}$$

is the angular frequency with which a ground observer standing in the SAR beam would see the platform crossing the sky. For high-flying satellites such as ERS,  $\omega_s$  is small and the nonlinearity parameter  $\Delta x/\lambda$  is large for most sea states.

The first simulations of the fully nonlinear velocity bunching mechanism for a random sea were achieved by mapping, pixel-by-pixel, the sea surface into the image plane, using a Monte Carlo simulation of the random wave height and associated orbital velocity fields (Alpers 1983, Alpers et al. 1986). This technique, however, is very expensive with respect to computing resources and does not lend itself readily to inversion, which is required to retrieve the wave spectrum from the measured SAR spectrum. It was not until the derivation by Hasselmann and Hasselmann (1991)—referred to in the following as HH-of a closed, nonlinear, spectral integral transform describing the mapping of the wave spectrum into the SAR image spectrum that the inversion problem was solved. The full integral can be expanded into a Taylor series with respect to orders of the nonlinearities in wave spectral components and velocity bunching. The individual terms represent Fourier transforms of higher order products of auto- and cross-covariance functions of RAR, hydrodynamic, and velocity bunching cross-section modulations, which may be efficiently computed with FFTs. Subsequently, Krogstad (1992) showed that the nonlinear transform could also be derived as the second-order moment of the characteristic function of a multivariate random vector that incorporates the local sea surface properties governing the SAR imaging of a moving sea surface. This framework also allowed generalizations (e.g., Krogstad et al. 1994; Engen and Johnsen 1995a).

## 1.5 Ocean wave spectral retrieval

Aspects of SAR imaging of ocean waves and the forward wave-to-SAR mapping relation have been validated for spaceborne SAR data recorded during Shuttle Imaging Radar (SIR) missions B and C, SIR-B/C (Alpers et al. 1986; Monaldo and Lyzenga 1988) and Russian spaceborne SAR mission ALMAZ-1 (anmas: Russian for diamond) (Wilde et al. 1994), as well as in the following airborne missions and field campaigns: Labrador Ice Margin Experiment, LIMEX (Raney et al. 1989); Labrador Extreme Waves Experiment, LEWEX (Beal 1991); Norwegian Continental Shelf Experiment, NORCSEX (Johnsen et al. 1991); Synthetic Aperture Radar and X-Band Nonlinearities—Forschungsplatform Nordsee, SAXON-FPN (Plant and Alpers 1994); Surface Wave Dynamics Experiment, SWADE (Cardone et al. 1995); Hasselmann et al. (1998b). The feasibility of retrieving wave spectra from SAR image spectra was demonstrated with SeaSat data (HH), aircraft data during LEWEX (Hasselmann et al. 1991), and ERS-1 data during the Grand Banks calibration and validation campaign (Grand Banks 1994).

The first detailed evaluation of the ERS-1 SAR wave mode was carried out for a three-day dataset in the Atlantic Ocean (Brüning et al. 1994a) and yielded an improved retrieval algorithm, WASAR (Hasselmann et al. 1996; referred to as HBHH). The square

deviation between the simulated and observed SAR image spectra, named cost function, is minimized iteratively. To reduce the cost function in wave spectral domain, the gradient  $\Delta F^n(\mathbf{k})$  is computed with the inverse of an explicit solution for the quasi-linear wave-to-SAR mapping,  $M^{ql}$ ,

$$\Delta F^n(\mathbf{k}) = (M^{ql})^{-1} \bullet P^n(\mathbf{k})$$

The updated SAR image spectrum  $P^{n+1}$  is inferred from the full closed nonlinear transform  $M^{nl}$  of the updated wave spectrum,

$$F^{n+1} = F^n + \Lambda F^n$$

The resolution of the 180° directional ambiguity inherent in frozen-image wave spectra is achieved using an additional term that penalizes deviations of the retrieved wave spectrum from the first-guess and favors the propagation direction corresponding to the first-guess direction. A third term penalizes deviations from the observed azimuthal cut-off wavenumber, which is a measure of the root-mean-square (rms) orbital velocity and, therefore, particularly sensitive to short waves beyond the cut-off wavenumber. In this manner it is possible to recover, at least in integral form, information on the short wavelength region of the wave spectrum that cannot be directly imaged.

Despite the explicit cut-off adjustment, the inversion method modifies the detailed form of the spectrum only in the main part of the spectrum, for which direct SAR spectral information is available. This difficulty is overcome in the HBHH algorithm by introducing a spectral partitioning scheme into the additional iteration loop that updates the input spectrum. The new input spectrum retains the continuity properties of the original input spectrum; however, the scales and propagation directions of the wave systems of the new spectrum are adjusted to the inverted spectrum.

A valuable feature of the WASAR algorithm is the availability of an internal calibration based on the level of background clutter spectrum. Thus, the retrieved spectrum can be calibrated in absolute wave height units without reference to the SAR instrument calibration or measurements of the absolute backscattering cross-section (Alpers and Hasselmann 1982; Brüning et al. 1994a). The WASAR algorithm is available from the German Climate Computing Centre in Hamburg (Hasselmann et al. 1998a).

An extensive assessment of the quality, performance, and sensitivity-related aspects of ERS-1 SWM data and the wave spectral retrieval procedure was carried out for the global 1993–1995 ERS-1 dataset (Heimbach et al. 1998; referred to as H3). Emphasis was also placed on the issue of first-guess dependence of the retrieved spectrum. A single or second iteration of the input spectrum yielded an appreciable improvement of the retrievals. Sensitivity experiments were conducted in which the first-guess was modified by changes in energy, frequency, and direction. For low and high wind speeds and for azi-

muth and range travelling waves, a statistical assessment of the modified retrievals showed only weak residual dependence of the retrieval on the first-guess input spectrum.

A complementary global validation of SWM-retrieved significant wave height,  $H_s$ , for 1994 was compared with independent, collocated, significant wave height data retrieved from the TOPEX and ERS-1 altimeters (Bauer and Heimbach 1999). Using the additional spectral information provided by the SWM partner of the collocated pairs, the full  $H_s$  sample was further stratified with respect to spectral properties. The SWM-retrieved swell wave heights were in particularly close agreement with altimeter-derived wave heights.

Various aspects of the inherent nonlinearities in the ERS-1 SWM product have been investigated using higher order spectral methods (e.g., Le Caillec et al. 1996; Kerbaol et al. 1998). SAR data from Canada's RadarSat have also been analyzed (Vachon et al. 1997a, 1997b).

#### 1.6 Wave data assimilation

Several techniques for assimilation of SAR wave spectral data into wave models have been developed. In all cases, both the wave spectra and the wind field are updated; the methods differed primarily in the level of sophistication and dynamical consistency.

#### Optimal interpolation

This technique, also called the nudging scheme, is straightforward to implement operationally. It was developed and applied to ERS-1 SWM wave spectral retrievals by Hasselmann et al. (1997).

## Green's function

This method incorporates more aspects of wave dynamics, in particular the propagation of swell, using a Green's function method developed by Bauer et al. (1996). In contrast to the optimal interpolation (OI) scheme, which yields only instantaneous wind corrections from the local wind-generated surface wave part of the spectrum, the Green's function method also derives corrections of past wind fields from the measured swell. The swell is traced to its origin by means of a two-dimensional wave age spectrum computed with an extended version of WAM. This greatly increases the proportion of wave measurements available for wind corrections. Although corrections of past wind data are of limited value for forecasting, they are useful for wind field reconstructions and statistical compilations. They also provide valuable information for wind field validation, particularly in intense wind regions that may be inadequately sampled by the normal observational network (see Section 2.2 and 3.2.3). The method also serves as a consistency check between wind corrections inferred from the local wind-generated surface waves, named windsea, and from swell.

#### Adjoint

The adjoint technique fully respects the model dynamics, rendering it the most dynamically consistent assimilation method. This fully variational approach was recently implemented in WAM with the Giering and Kaminski (1998) tangent linear and adjoint model compiler (TAMC). However, the adjoint method is expensive with respect to computing time and has been applied only for model tuning (Hersbach 1998), not for assimilation of satellite data.

## 2. Global Comparison of ERS-1 SWM and WAM Wave Spectra

The section addresses applications of ERS-1 SAR wave spectral retrievals for model validation and investigations of large-scale fields of two-dimensional wave spectral properties. We also present a validation of the WAM model using ERS-1 SWM data that differs from that presented in H3, because WAM was re-run without assimilation of ERS-1 altimeter data.

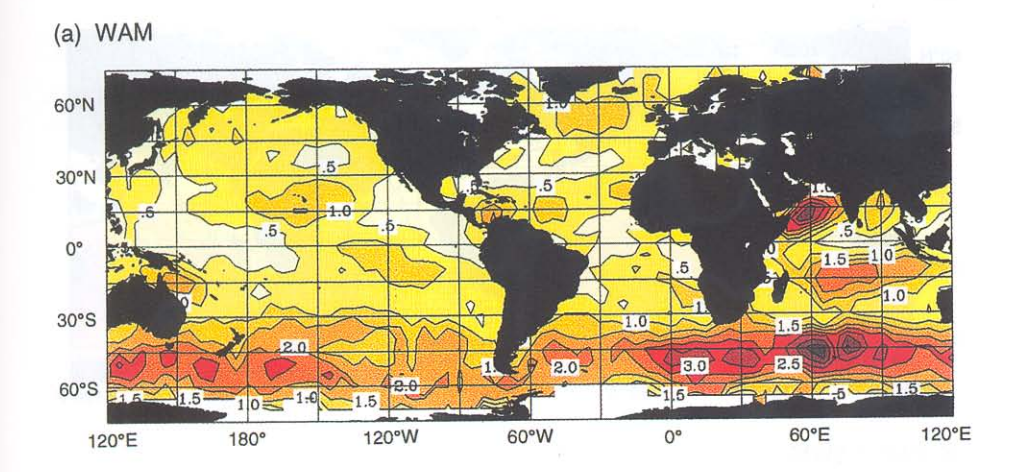
## 2.1 Global distribution of seasonal mean spectral properties

Monthly and seasonal mean spectral properties retrieved from 1993 to 1995 ERS-1 SWM data and from WAM, produced operationally at ECMWF, have been compared by H3. Figures 1 and 2 show examples of global distributions of seasonal mean windsea and swell wave heights, respectively, for austral winter June–August 1994. The selection criteria for swell focused on low-frequency swell. Thus, the distributions refer only to the largest swell components within each spectrum, and only swell with wavelength greater than 250 m is included; the partitioning scheme used to define the swell components is described in HBHH. The windsea distributions (Figure 1) reflect the seasonal properties of atmospheric circulation, with maxima in the Southern Hemisphere mid-latitude westerly storm belt. The influence of the trade winds is clearly seen in the tropics, while strong monsoon-driven windsea systems are found in the Arabian Sea (Figure 1). As discussed by H3, the WAM slightly overpredicts windsea wave heights. This is attributed to the strength of ECMWF winds, a contention that is supported by a comparison between ECMWF and ERS-1 scatterometer-derived wind fields (Bentamy et al. 1996).

The large-scale pattern of swell (Figure 2) differs from the windsea distribution (Figure 1). Swell radiates along great circles from the main source regions in the Southern Hemisphere mid-latitudes towards the east and the tropics. Shadowing by continents is also apparent. In contrast to the windsea, swell wave heights are systematically underpredicted by the WAM, which appears to have excessive damping (H3).

# 2.2 Comparison of model simulations with and without assimilation

To avoid a possible spurious bias introduced into the operational ECMWF wave spectral analysis through the assimilation of ERS-1 altimeter significant wave heights (H3),





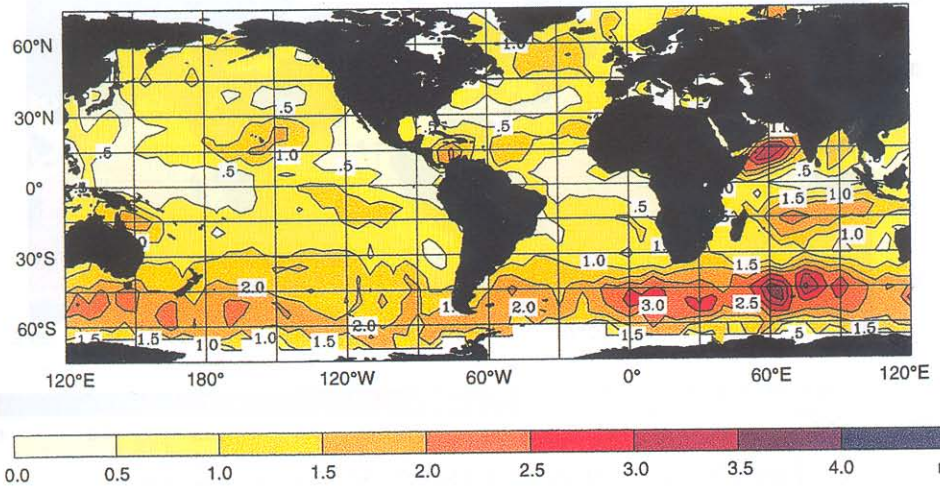
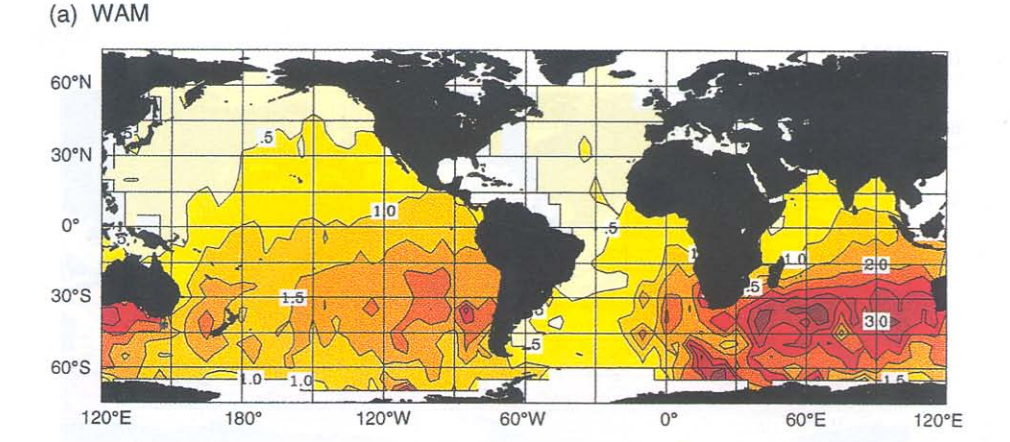


**Figure 1.** (a) WAM and (b) ERS-1 SWM seasonal mean windsea wave heights for June–August 1994.

the WAM for June-August 1995 was re-computed without assimilation of these data. The computational setup and wind forcing were identical to the operational configuration at ECMWF. A comparison of the ERS-1 SWM retrievals with the model simulations performed with and without assimilation of ERS-1 altimeter data confirms the qualitative conclusions described by H3. However, the magnitudes of the differences between the modeled and retrieved windseas and swell are affected by assimilation of the altimeter data (Figure 3).



#### (b) ERS-1 SWM

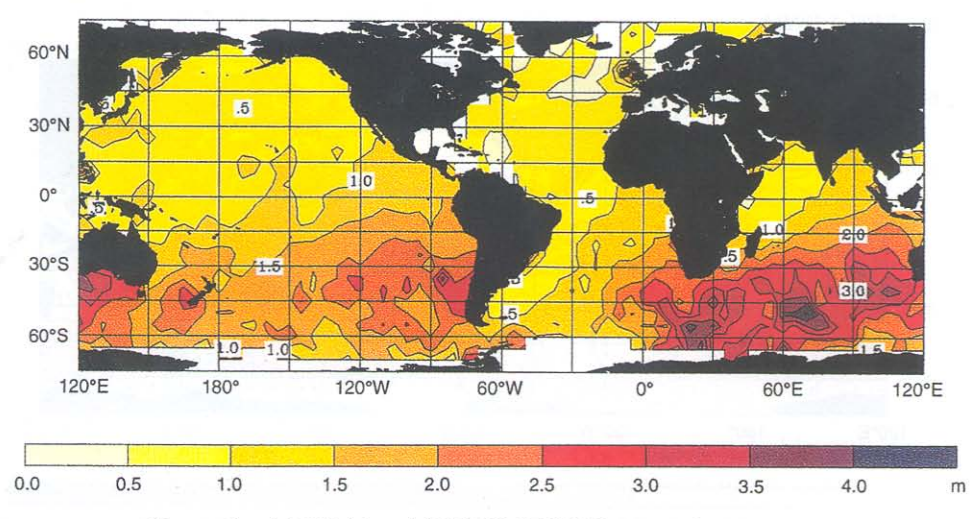


**Figure 2.** (a) WAM and (b) ERS-1 SWM seasonal mean wave height distributions of individual largest wavelength swell systems of wavelengths exceeding 250 m for June–August 1994.

Bauer and Heimbach (1999) reported that the ERS-1 altimeter data appear to be systematically low biased since January 1994. Thus, both mean windsea and swell wave heights for the WAM simulation without assimilation exceed the ECMWF data with assimilation. However, the effect is much smaller for windsea than for swell (Figure 3); swell covers a much larger area in the ocean than windsea and is, therefore, more frequently updated. The optimal interpolation assimilation scheme implemented at ECMWF updates windsea only when the satellite passes over the relatively limited storm area. This is a far more unlikely occurrence than updating a swell that has left the storm

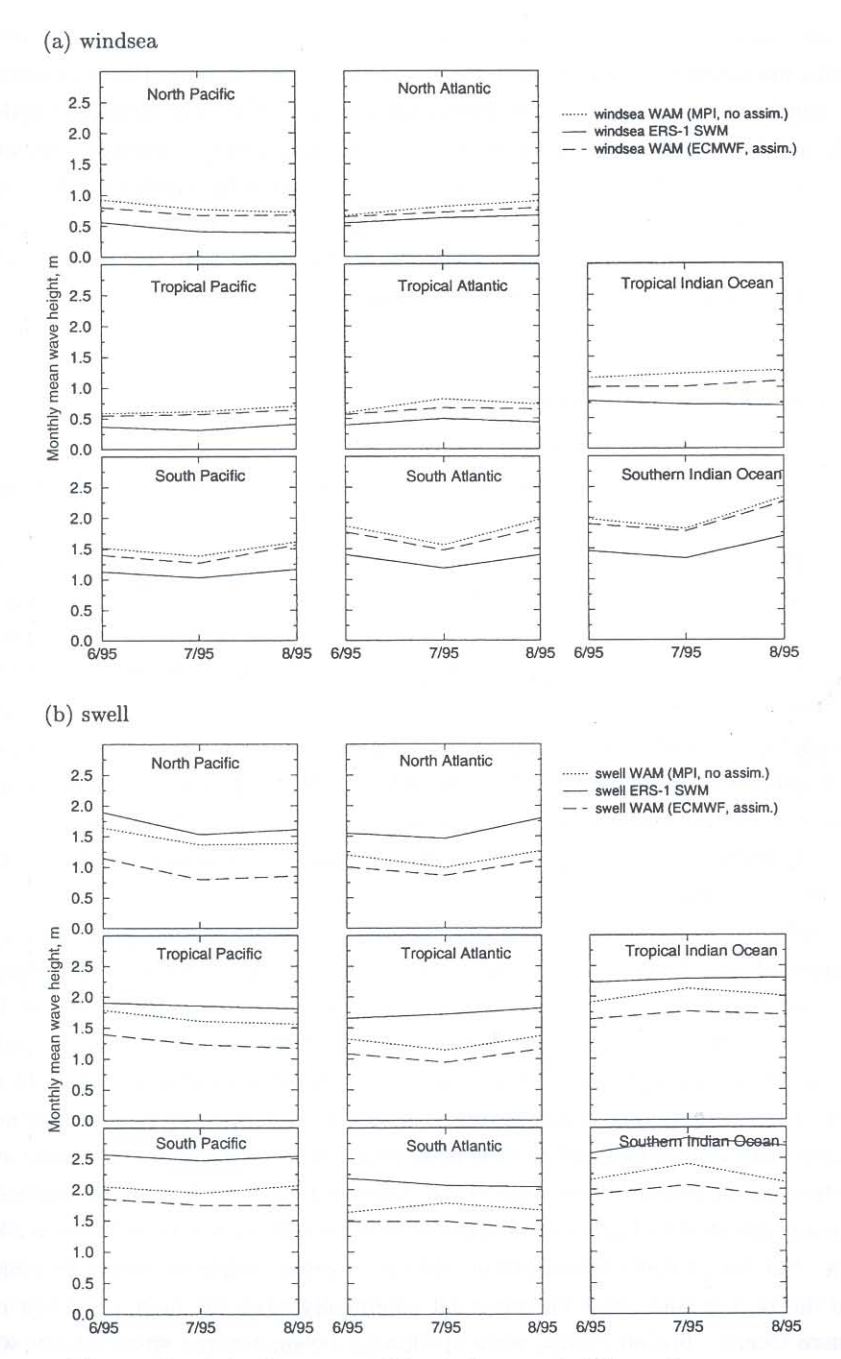


**Figure 3.** Monthly mean (a) windsea and (b) swell wave heights for ERS-1 SWM, WAM with assimilation (long dashed line), and WAM without assimilation (dotted line) in different ocean basins for June–August 1995.

area, and can be detected repeatedly several days later over an expanding area. This also explains the limited impact of wind corrections from the OI assimilation of significant wave height data (e.g., Breivik et al. 1998; Dunlap et al. 1998). The number of updates is small, and the updates for which windsea can be unambiguously separated from swell in the single, integral wave height provided by the altimeter is too small to make a significant impact (Sections 1.6 and 3.2). Although the sign is maintained, the bias in the swell is reduced by one-third to one-half, depending on the ocean basin, for the case without assimilation compared to the case with assimilation.

## 3. Trans-Ocean Propagation of Swell

## 3.1 Snodgrass et al. (1966) experiment

Sverdrup and Munk (1947), Barber and Ursell (1948), and Munk and Snodgrass (1957) indicated the ability of swell to travel over very large distances across ocean basins. During the austral winter of 1963, the first major ocean wave experiment was carried out to measure the propagation of swell across the Pacific Ocean (Snodgrass et al. 1966). The main goal was to determine whether, by how much, and by what mechanism swell was attenuated over a long path. Data would be used to test the Phillips (1957) and Miles (1957) theories of wave generation by wind, and the transfer of energy across the spectrum by resonant nonlinear interactions among ocean waves which generates long wavelength swell (Hasselmann 1967). In addition, the spectral action balance equation provided an elegant framework for propagation of swell wave packets along great circle rays on a sphere, viewed as a problem of Hamiltonian ray dynamics. Little was known about the dissipation of ocean swell.

To infer the source of long swell and estimate its travel time, Snodgrass et al. (1966) concentrated on a 'great-circle' in the Pacific, along which several wave-recording stations were installed. The 'reference great-circle' was chosen at an inclination of 195.5° with respect to Honolulu and connected regions of high storms east of New Zealand with the coast of Alaska at Yakutat. Snodgrass et al. (1966) were able to detect 12 major events. Their main finding was that long wavelength swell (λ >280 m), once the nonlinear wave-wave interactions had become negligible, propagated without detectable attenuation beyond the immediate vicinity of the generation region. A weak attenuation was marginally detected for large wave height swell events with wavelengths between 240 and 280 m. For wavelengths below 240 m, individual events could no longer be identified above the background swell radiating out continually from the high wind belt of the Southern Ocean. For all events, wave shadowing by intervening small islands was an important consideration that complicated the computed attenuation. Contributing to scatter in the observed attenuation were differences in the geometry and intensity of the wind fields of individual storm events.

In the next section, we examine swell propagation over very large distances, making use of the greatly expanded database provided by ERS-1 SAR wave mode data. Although the satellite cannot provide continuous time series at specific locations, it does yield global, quasi-continuous coverage, enabling various stages of the travelling swell to be observed at many locations and times.

#### 3.2 The 4-6 June 1995 South Pacific storm

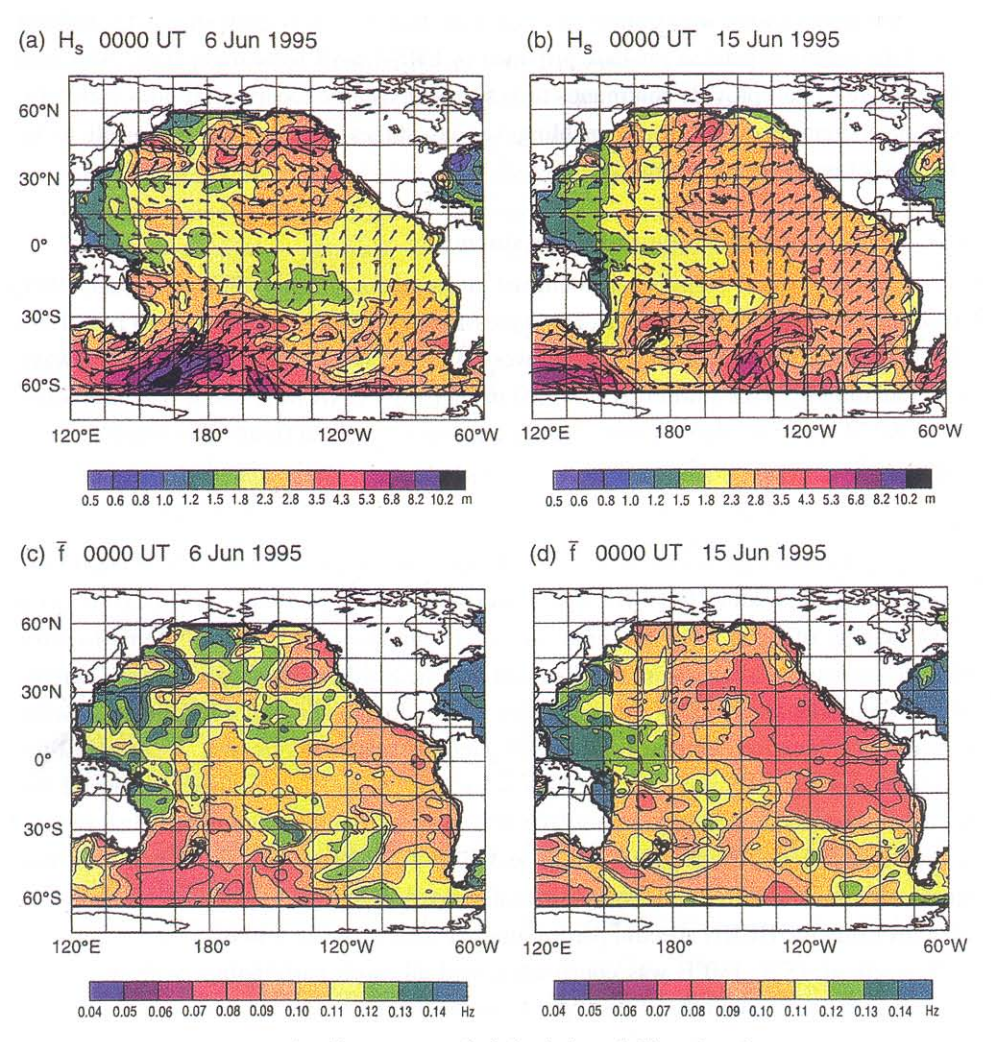
An extreme storm event began southeast of Tasmania (60°S, 145°E) on 4 June 1995. According to the ECMWF analysis, a low pressure system at 55°S, 165°E on 6 June 1995 slowly moved eastward, producing southwesterly wind speeds up to 20 m s<sup>-1</sup>. The wave field radiating from the storm was analyzed using ERS-1 SAR wave-mode data and collocated WAM spectral values of wave energy and wave age at all frequency-direction spectral bins (Bauer et al. 1996).

#### Wave field

Figure 4a shows the vector field of significant wave height in the Pacific at 0000 Universal Time (UT) 6 June 1995. The dominant feature is the pronounced storm center, with wave heights of 12 m. At that time, no significant wave propagation seems to have occurred across the tropics from the Southern into the Northern Hemisphere: wave heights in the tropics remained below 2 m, and wave vectors followed more or less the local wind pattern. The situation changed considerably nine days later (Figure 4b). A northwest-to-southeast oriented ridge of 2.8- to 3.5-m wave heights with wave direction toward the northeast occurred 1000–2000 km off North America, extending into the tropical region. To select a collocated sample of WAM and ERS-1 SWM spectra associated with this storm, all available WAM and SWM-retrievals were decomposed into their principal wave systems using the HBHH spectral partitioning algorithm. A fan grid of 'great-circle' rays with origin at 45°S, 180°E was constructed, and all swell partitionings with directions aligned within ±30° with the nearest 'great-circle' direction were selected.

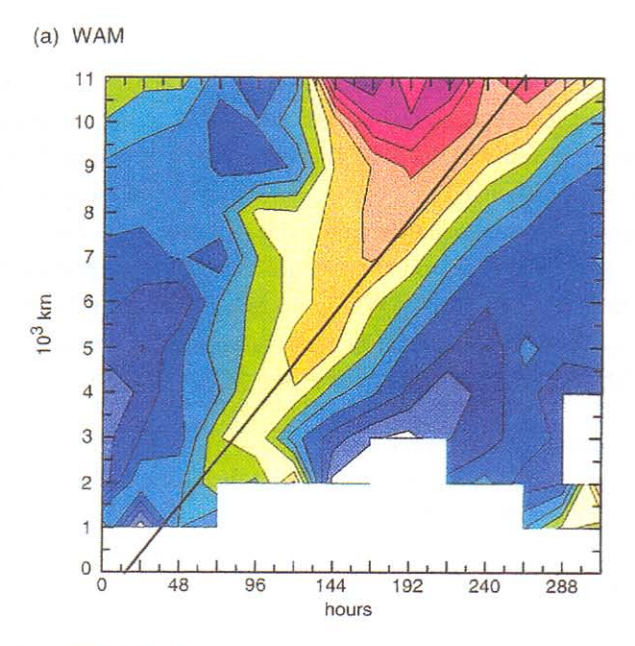
## Wavelength-propagation diagram

To investigate variations in wavelength with position and time for the swell, a travel-time and distance diagram or Hovmüller diagram was constructed for WAM and SWM swell partitionings. Both ERS-1 SWM and WAM display (Figure 5) the propagation of a long wavelength signal along a ridge of maximum wavelength. The wavelength along the ridge increases with increasing distance and travel time. Moreover, a broadening and slight positive curvature of the ridge, with increasing distance from the generating storm, occurred. Both the increase in wavelength with increasing distance from the source and the positive curvature are consistent with the selective attenuation of shorter swell, leaving behind longer swell components with higher speed. This is also consistent with the effect of wave dispersion, in which long waves travel faster than short waves. Thus, the ridge



**Figure 4.** Significant wave height (m) and direction (top panels) and mean frequency (Hz) (bottom panels) on (a, c) 6 June 1995 and (b, d) 15 June 1995, both at 0000 UT.

bends upwards from the constant slope line, which would correspond to a constant mean frequency of the swell system. Faster waves with larger wavelengths appear first at a specific location. WAM had a broader ridge compared with SWM because of the numerical dispersion of the first-order upwind propagation scheme used in WAM. Although the propagation scheme conserves energy, barely impacting the overall wave statistics, for the coarse 30° directional resolution used by the ECMWF operational model, this characteristic must be taken into account when studying individual propagation events.



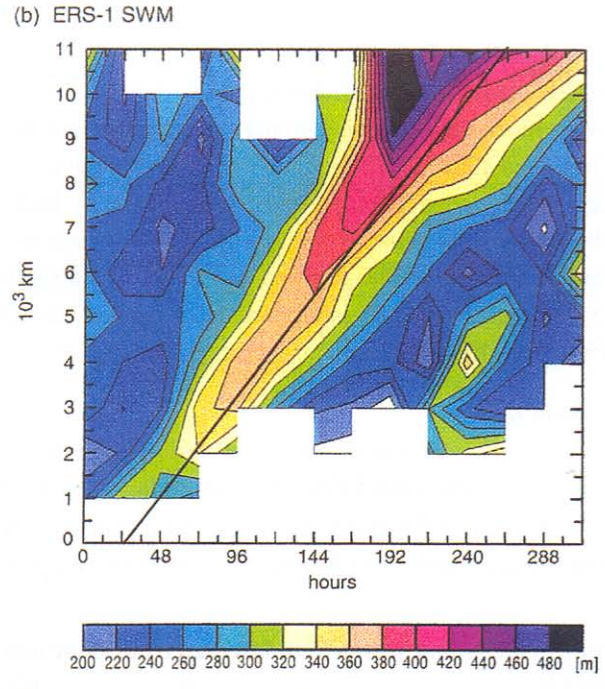


**Figure 5.** Travel time and distance diagram for (a) WAM and (b) ERS-1 SWM data showing wavelengths with respect to a reference time of 0000 UT 6 June 1995 and a reference location of 55°S, 165°E.

The slope of the maximum wavelength ridge (Figure 5) is the group velocity of the dominant swell. This allows the associated wavelength to be inferred from the dispersion relation, yielding an independent wavelength estimate that can be compared with the modeled or measured local wavelength. The slope may be computed locally at various points along the ridge, idealized as a curve, and compared to the observed wavelength. The only requirement for the slope to be detectable is for the local wavelength to be larger than the wavelength of the background swell (i.e., the ridge is significant relevant to the background). The WAM and ERS-1 SWM group velocities (Table 2) were in good agreement. However, the WAM significantly underestimated the wavelength compared to ERS-1 SWM (Table 2), which is discussed below.

## Ray back-tracing using spectral wave age

To focus on long wavelength swell, we restrict the collocated swell dataset to waves with wavelengths above 300 m. We then trace the path of the swell from observed positions to position and time of origin using the locally determined spectral wave age, wavelength, and propagation direction to reconstruct each 'great-circle' propagation path. WAM results (Figure 6c) show the west-to-east shift of the generation area, in accord with the movement of the storm center. The spectral wave age is clearly a useful variable for classifying swell history and should be incorporated into wave models, such as the dynamically consistent data assimilation scheme proposed by Bauer et al. (1996).

ERS-1 SAR wave mode data along individual 'great-circles' are very scattered (Figure 6b), perhaps by island shadowing (Snodgrass et al. 1966), numerical dispersion that result in inaccuracies along individual rays, and contamination by background swell not associated with the storm. It is unlikely that inaccurate SWM data and the partitioning scheme to determine the swell wavelengths and wave heights are significant sources of scatter, because SWM data were successfully validated against altimeter wave heights (e.g., Bauer and Heimbach 1999).

## Wind field in the storm region

WAM swell wavelengths are considerably lower than the wavelengths of ERS-1 retrievals (Table 2). This suggests that ECMWF wind forcing is too weak compared with actual winds. In an analysis of South Pacific wave data, H3 conjectured that ECMWF underestimated wind speed south of 50°S. We also tested the hypothesis of underesti-

Table 2. Group velocity and wavelength inferred from slope and main ridges in Figure 6.

-	Slope (= group velocity)	Wavelength (inferred from slope)	Wavelength (inferred from ridge)		
WAM	12.1 m s <sup>-1</sup>	375 m	340-380 m		
ERS-1 SWM	$13.4 \text{ m s}^{-1}$	460 m	420-460 m		

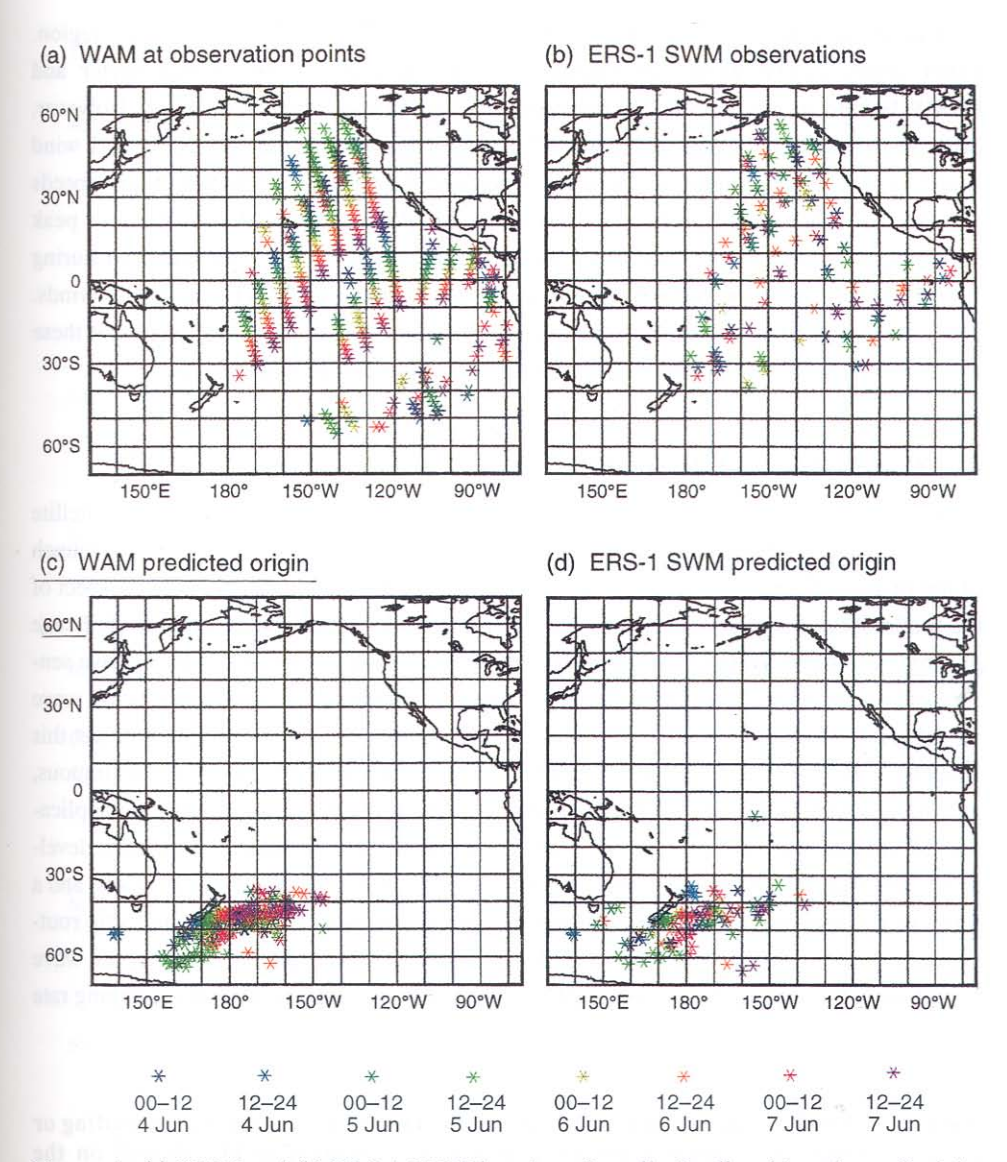


**Figure 6.** (a) WAM and (b) ERS-1 SWM location of swell. Predicted locations of origin of swell from (c) WAM and (d) ERS-1 SWM data, within ±2 days of 00 UT 6 June 1995.

mated ECMWF winds in the intense storm region by a direct comparison with wind vectors retrieved from the ERS-1 scatterometer. The storm area is about 45°–70°S and 140°–180°E. Between 0000 UT 5 June and 1800 UT 6 June 1995, the area was overflown six times by ERS-1. Only overflights 3 and 5 had footprints passing close to the storm center (Table 3) because wind directions were about 225° (Figure 7a), i.e., normal to the mean

windsea direction (045°) inferred from the swell propagating away from the storm region. Other orbits exhibit higher differences in wind directions. The scatterometer and ECMWF wind speeds (Figure 7b) for overflight 3 are in reasonable agreement. However, orbit 5 exhibits large deviations between ECMWF and ERS-1 wind speeds. ERS-1 wind speeds reach a maximum of 29 m s<sup>-1</sup>, one-third larger than ECMWF wind speeds (Figure 7b). These data provide evidence that ECMWF analysis did not resolve peak wind speeds of the storm. For wind speeds below about 20 m s<sup>-1</sup> encountered during overflights 1, 2, 4, and 6, there is no systematic bias between ECMWF and ERS-1 winds. The lower wind speeds relative to the peak values observed on orbit 5 confirm that these overflights passed close to, but not through, the high wind center of the storm.

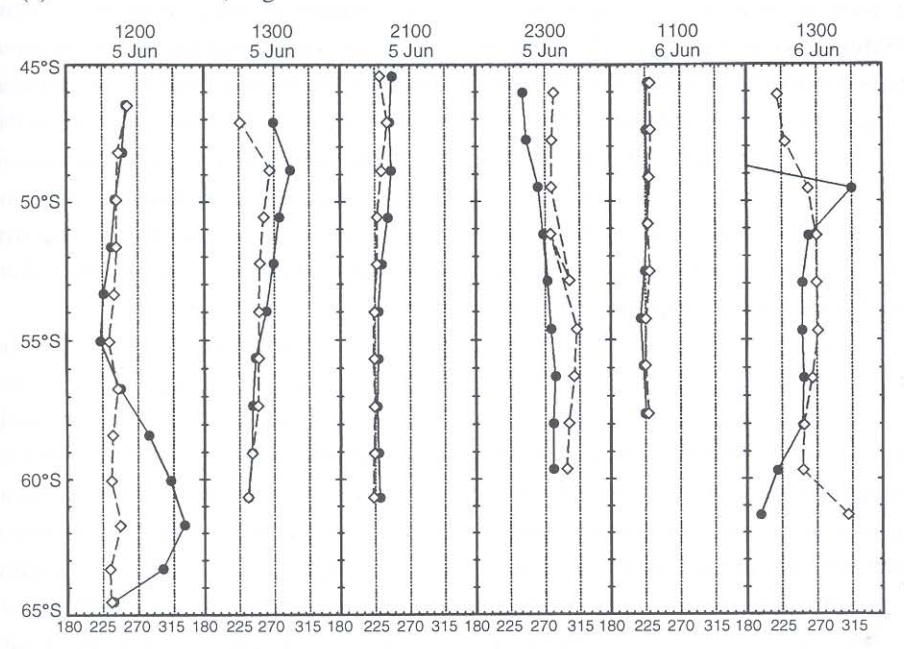
## 4. Conclusions and Perspectives

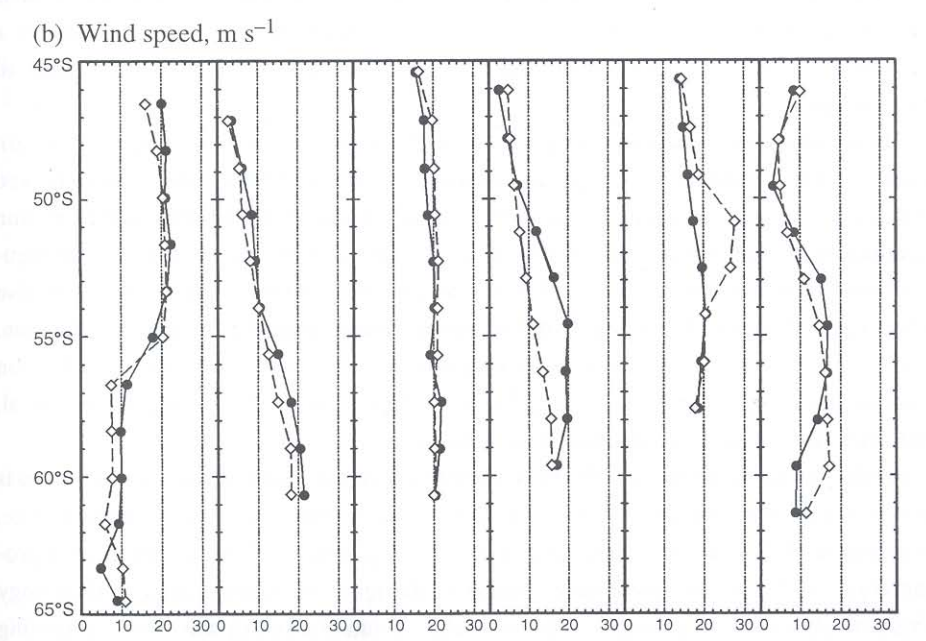
Research and modeling of ocean waves and the development and application of satellite remote-sensing methods for ocean waves have made remarkable progress since the launch of the first ocean satellite, SeaSat, more than 20 years ago. Before SeaSat, the prospect of the availability of global wave height and two-dimensional spectral data, and the challenge of retrieving that data from complex—and as yet inadequately validated—microwave sensor systems, provided a major stimulus for research. Sophisticated third-generation wave models and complex SAR wave-spectral retrieval algorithms were developed to meet this challenge. By the time ERS-1 was launched 13 years later in 1991, providing continuous, global, near-real-time wave data for the first time, most of the techniques for the application of satellite wave data for research and operational wave forecasting had been developed. The following years have seen a validation of the basic techniques and models, and a series of interesting applications for research, operational wave forecasting, and ship routing optimization (Lehner et al. 1996). ERS data have also been used to detect ocean wave refraction in the marginal ice zone, and to quantify sea ice thickness from the damping rate (Schulz-Stellenfleth et al. 1999; Schulz-Stellenfleth and Lehner 1999).

Table 3. ERS-1 overflights over the storm area. Orbits were either (a) ascending or (d) descending. Individual orbit footprints were estimated to be situated on the forward face, in the center, or on the backward face of the storm.

Number	Day	Time interval	Orbit	Longitude	Position relative to storm center
1	95/06/05	12:14-12:20	a	165°E-180°	forward
2	95/06/05	13:56-14:01	a	140°E-149°E	back
3	95/06/05	21:59-22:04	d	164°E-174°E	center
4	95/06/05	23:41-23:45	d	140°E-149°E	back
5	95/06/06	11:45-11:49	a	172°E-180°	center
6	95/06/06	13:25-13:29	a	148°E-158°E	back







**Figure 7.** (a) Wind direction and (b) wind speed from ERS-1 scatterometer (dashed line) and ECMWF analysis (solid line) along ERS-1 ground tracks over the storm area.

However, much remains to be done. Interactions between operational wave forecasting, wave research, and satellite ocean wave remote sensing should be intensified. While operational ocean wave forecasts are being used successfully to provide first-guess inputs for the operational retrieval of SAR wave spectral data, the assimilation of these retrievals for operational wave forecasting has yet to be implemented. Existing operational data assimilation techniques are limited to relatively simple optimal interpolation methods for altimeter wave height data, which, as single integral values with undefined partitioning between windsea or swell, can have only a limited, imprecise impact on wave and wind updates. Assimilation schemes for SAR wave spectral retrievals have been validated and should now be tested in operational forecasts.

Another important area of development is the construction of coupled ocean-atmosphere models with a wave model, such as the European Coupled Atmosphere Wave Ocean Model (Weisse and Alvarez 1997). A coupled ocean-atmosphere model with a dynamical interface would be valuable for weather, wave, and storm surge forecasting (Mastenbroek et al. 1993; Weber et al. 1993), for seasonal and interannual climate forecasts, and for scenario computations of anthropogenic climate change. This type of model would be particularly relevant for predicting the statistics of extreme events, which are becoming increasingly important in the context of natural climate variability and anthropogenic climate change (WASA Group 1998). Comprehensive coupled models will also be needed for advanced data assimilation schemes that strive to achieve a dynamically consistent, simultaneous update of all relevant coupled fields, using all available data.

There continues to be room for progress in the area of sensors and algorithms. An example is the development and operational implementation in ENVISAT of an improved SAR wave cross-spectral retrieval system that makes use of the additional information contained in the individual looks of a multi-look SAR image to remove the 180° ambiguity of current frozen-image spectra (Johnsen and Desnos 1999). Improvements are also to be expected in the formulation of the hydrodynamic modulation transfer function. Research is directed towards a better description of shortwave-to-longwave modulation (Kudryasvtsev et al. 1997), including the wind dependence (Plant 1982; Feindt et al. 1986; Hara and Plant 1994; Brüning et al. 1994b).

Finally, essential to the success of a satellite ocean wave remote-sensing program is the maintenance of continuous, long-term global observations. The achievements to date, beginning with SeaSat and continuing with ERS-1/2, must still be regarded as a prolonged proof-of-concept, while development of the requisite sophisticated methodology is very much a work in progress. The real value of satellite ocean wave remote sensing will be realized when the techniques have been fully implemented in operational wave forecasting, the data are routinely used in research, and the observational time series have become sufficiently long to be used in global change studies.

Acknowledgments. In addition to new results, this paper reviews work carried out by the authors with Susanne Hasselmann and Eva Bauer, whose contributions are gratefully acknowledged. The work was supported in part by grants N00014-92-J-1840 and N00014-1-0541 from the U.S. Office of Naval Research (ONR), through the SFB-318 project funded by the Deutsche Forschungsgemeinschaft (DFG), and through the European Space Agency (ESA) pilot project PP2.D1.

#### References

- Alpers, W., and K. Hasselmann, The two-frequency microwave technique for measuring ocean wave spectra from an airplane or satellite, *Bound. Layer Meteorol.*, 13, 215–230, 1978.
- Alpers, W., and C. L. Rufenach, The effect of orbital motions on synthetic aperture radar imaging of ocean waves, *IEEE Trans. Antennas Propag.*, 27, 685–690, 1979.
- Alpers, W., and K. Hasselmann, Spectral signal-to-clutter and thermal noise properties of ocean wave imaging synthetic aperture radars, *Int. J. Remote Sensing*, *3*, 423–446, 1982.
- Alpers, W., D. B. Ross, and C. L. Rufenach, On the detectability of ocean surface waves by real and synthetic aperture radar, *J. Geophys. Res.*, 86, 6481–6498, 1981.
- Alpers, W., C. Brüning, and K. Richter, Comparison of simulated and measured synthetic aperture radar image spectra with buoy-derived ocean wave spectra during the Shuttle Imaging Radar-B mission, *IEEE Trans. Geosci. Remote Sensing*, 24, 559–566, 1986.
- Atanasov, V., W. Rosenthal, and F. Ziemer, Removal of ambiguity of two-dimensional power spectra obtained by processing ship radar images of ocean waves, *J. Geophys. Res.*, 90, 1061–1067, 1985.
- Barber, B. F., and F. Ursell, The generation and propagation of ocean waves and swell: I. Wave periods and velocities, *Phil. Trans. Roy. Soc. Lond. A*, 240, 527–560, 1948.
- Bauer, E., and P. Heimbach, Annual validation of significant wave heights of ERS-1 synthetic aperture radar wave mode spectra using TOPEX/Poseidon and ERS-1 altimeter data, *J. Geophys. Res.*, 104, 13345–13357, 1999.
- Bauer, E., K. Hasselman, I.R. Young, and S. Hasselmann, Assimilation of wave data into the wave model WAM using an impulse response function, *J. Geophys. Res.*, 101, 3801–3816, 1996.
- Beal, R. C., editor, *Directional Ocean Wave Spectra*, The Johns Hopkins University Press, Baltimore, 1991.
- Bentamy, A., N. Grima, Y. Quilfen, V. Harscoat, C. Maroni, and S. Pouliquen, An atlas of surface wind from ERS-1 scatterometer measurements 1991–1996, Technical Report, IFREMER/CERSAT, Plouzané, France, 1996.
- Breivik, L.-A., M. Reistad, H. Schyberg, J. Sunde, H. E. Krogstad, and H. Johnsen, Assimilation of ERS SAR wave spectra in an operational wave model, *J. Geophys. Res.*, 103, 7887–7900, 1998.
- Brüning, C., W. Alpers, and J. Schröter, On the focusing issue of synthetic aperture radar imaging of ocean waves, *IEEE Trans. Geosci. Remote Sensing*, 29, 120–128, 1991.
- Brüning, C., S. Hasselmann, K. Hasselmann, S. Lehner, and T. W. Gerling, A first evaluation of ERS-1 synthetic aperture radar wave mode data, *Global Atmos. Ocean System*, 2, 61–98, 1994a.

- Brüning, C., R. Schmidt, and W. Alpers, Estimation of the ocean wave—radar modulation transfer function from synthetic aperture radar imagery, *J. Geophys. Res.*, 99, 9803–9816, 1994b.
- Cardone, V. J., H. C. Graber, R. E. Jensen, S. Hasselmann, and M. J. Caruso, In search of the true surface wind field in SWADE IOP-1: Ocean wave modeling perspective, *Global Atmos. Ocean System*, *3*, 107–150, 1995.
- Cardone, V. J., R. E. Jensen, D. T. Resio, V. R. Swail, and A. T. Cox, Evaluation of contemporary ocean wave models in rare extreme events: The "Halloween Storm" of October 1991 and the "Storm of the Century" of March 1993, *J. Atmos. Oceanic Tech.*, 13, 198–230, 1996.
- Chapron, B., T. Elfouhaily, and V. Kerbaol, Calibration and validation of ERS Wave Mode products, DRO/OS/95-02, IFREMER/CERSAT, Plouzané, France, 1995.
- Dunlap, E. M., R. B. Olsen, L. Wilson, S. De Margerie, and R. Lalbeharry, The effect of assimilating ERS-1 fast delivery wave data into the North Atlantic WAM model, *J. Geophys. Res.*, 103, 7901–7915, 1998.
- Engen, G., and H. Johnsen, SAR ocean wave inversion using image cross-spectra, *IEEE Trans. Geosci. Remote Sensing*, *33*, 1047–1056, 1995a.
- Engen, G., and H. Johnsen, Analysis and inversion of ERS-1 image cross-spectra, In Proc. IGARSS'95, IEEE Press, Piscataway, NJ, 1863–1865, 1995b.
- Feindt, F., J. Schröter, and W. Alpers, Measurement of the ocean wave—radar modulation transfer function at 35 GHz from a sea-based platform in the North Sea, *J. Geophys. Res.*, 91, 9701–9708, 1986.
- Giering, R., and T. Kaminski, Recipes for adjoint code construction, *ACM Trans. Math. Software*, 24, 437–474, 1998.
- Gower, J. F. R., "Layover" in satellite radar images of ocean waves, *J. Geophys. Res.*, 88, 7719–7720, 1983.
- Grand Banks, The Grand Banks ERS-1 SAR Wave Spectra Validation Experiment, *Atmos.-Ocean*, 32, 3–256, 1994.
- Hara, T., and W. R. Plant, Hydrodynamic modulation of short wind-wave spectra by long waves and its measurement using microwave backscatter, *J. Geophys. Res.*, *99*, 9767–9784, 1994.
- Hasselmann, K., Nonlinear interactions treated by the methods of theoretical physics (with application to the generation of waves by the wind), *Phil. Trans. Roy. Soc. Lond. A*, 299, 77–100, 1967.
- Hasselmann, K., A simple algorithm for the direct extraction of the two-dimensional surface image spectrum from the return signal of a synthetic aperture radar, *IEEE Trans. Geosci. Remote Sensing*, 1, 219–240, 1980.
- Hasselmann, K., and Hasselmann, S., On the nonlinear mapping of an ocean wave spectrum into a synthetic aperture radar image spectrum and its inversion, *J. Geophys. Res.*, *96*, 10713–10729, 1991.
- Hasselmann, K., R. K. Raney, W. J. Plant, W. Alpers, R. A. Shuchman, D. R. Lyzenga, C. L. Rufenach, and M. J. Tucker (MARSEN Group), Theory of synthetic aperture radar ocean imaging: A MARSEN view, *J. Geophys. Res.*, 90, 4659–4686, 1985.
- Hasselmann, K., S. Hasselmann, C. Brüning, and A. Speidel, Interpretation and application of SAR wave image spectra in wave models, In *Directional Ocean Wave Spectra*, edited by R. Beal, The Johns Hopkins University Press, Baltimore, 117–124, 1991.
- Hasselmann, S., P. Heimbach, and C. Bennefeld, The WASAR algorithm for retrieving ocean wave spectra from SAR image spectra, Technical Report 14, Deutsches Klimarechenzentrum (DKRZ), Hamburg, 1998a.

- Hasselmann, S., P. Lionello, and K. Hasselmann, An optimal interpolation assimilation scheme for wave data, *J. Geophys. Res.*, 101, 16615–16629, 1997.
- Hasselmann, S., C. Brüning, K. Hasselmann, and P. Heimbach, An improved algorithm for the retrieval of ocean wave spectra from SAR image spectra, *J. Geophys. Res.*, 101, 16615–16629, 1996.
- Hasselmann, S., C. Bennefeld, H. Graber, D. Hauser, F. Jackson, P. Vachon, E. J. Walsh,
  K. Hasselmann, and R. B. Long, Intercomparison of two-dimensional wave spectra
  obtained from microwave instruments, buoys and WAModel simulations during the
  Surface Wave Dynamics Experiment, Report 258, MPI für Meteorologie, Hamburg,
  1998b.
- Heimbach, P., S. Hasselmann, and K. Hasselmann, Statistical analysis and intercomparison of WAM model data with global ERS-1 SAR Wave Mode spectral retrievals over three years, *J. Geophys. Res.*, 103, 7931–7978, 1998.
- Hersbach, H., Application of the adjoint of the WAM model to inverse wave modeling, J. Geophys. Res., 103, 10469–10487, 1998.
- Hφgda, K. A., G. Engen and H. Johnsen, Wind field estimation from SAR ocean images, In Proc. IGARSS'98, IEEE Press, Piscataway, NJ, 1998.
- Jain, A., Focusing effects in the synthetic aperture radar imaging of ocean waves, *App. Phys.*, 15, 323–333, 1978.
- Janssen, P. A. E. M., and P. Viterbo, Ocean waves and the atmospheric climate, *J. Climate*, *9*, 1269–1287, 1996.
- Johannessen, J. A., E. Attema, and Y.-L. Desnos, Wind field retrieval from SAR, Earth Observation Quarterly EOQ No. 59, European Space Agency, ESA Publications Division, ESTEC, Noordwijk (NL), 1998.
- Johnsen, H., Multi-look versus single-look processing of synthetic aperture radar images with respect to ocean wave spectra estimation, *Int. J. Remote Sensing*, 13, 1627–1643, 1992.
- Johnsen, H., and Y.-L. Desnos, Expected performance of ENVISAT ASAR wave mode product, In Proc. IGARSS'99, IEEE Press, Piscataway, NJ, 1999.
- Johnsen, H., K. A. Hφgda, T. Guneriussen, and J. P. Pedersen, Azimuth smearing in synthetic aperture radar ocean image spectra from the Norwegian Continental Shelf Experiment of 1988, *J. Geophys. Res.*, 96, 10443–10452, 1991.
- Junger, S., The Perfect Storm, W. W. Norton and Company, New York, 227 pp, 1997.
- Kasilingam, D. P., and O. H. Shemdin, Theory for synthetic aperture radar imaging of the ocean surface: With application to the tower ocean wave and radar dependence experiment on focus, resolution, and wave height spectra, *J. Geophys. Res.*, 93, 13837–13848, 1988.
- Kerbaol, V., B. Chapron, and P. W. Vachon, Analysis of ERS-1/2 synthetic aperture radar wave mode imagettes, *J. Geophys. Res.*, 103, 7833–7846, 1998.
- Komen, G. J., L. Cavaleri, M. Donelan, K. Hasselmann, S. Hasselmann, and P. A. E. M. Janssen, *Dynamics and Modeling of Ocean Waves*, Cambridge University Press, Cambridge, 560 pp, 1994.
- Krogstad, H. E., A simple derivation of Hasselmann's nonlinear ocean-synthetic aperture radar transform, *J. Geophys. Res.*, *97*, 2421–2425, 1992.
- Krogstad, H. E., O. Samset, and P. W. Vachon, Generalization of the nonlinear ocean-SAR transform and a simplified SAR inversion algorithm, *Atmos.-Ocean*, 32, 61–82, 1994.
- Kudryavtsev, V. N., C. Mastenbroek, and V. K. Makin, Modulation of wind ripples by long surface waves via the air flow: a feedback mechanism, *Bound. Layer Meteorol.*, 83, 99–116, 1997.

Le Caillec, J. M., R. Garello, and B. Chapron, Two dimensional bispectral estimates from ocean SAR images, Nonlin. Proc. Geophys., 3, 196-215, 1996.

Lehner, S., T. Bruns, and K. Hasselmann, Test of a new onboard ship routing system, In Proc. Second ERS Applications Workshop, ESA SP-383, ESA Publications Division, ESTEC, Noordwijk (NL), 297-301, 1996.

Lehner, S., J. Horstmann, W. Koch, and W. Rosenthal, Mesoscale wind measurements using recalibrated ERS SAR images, J. Geophys. Res., 103, 7847-7856, 1998.

Lyzenga, D. R., An analytic representation of the synthetic aperture radar image spectrum for ocean waves, J. Geophys. Res., 93, 13859-13865, 1988.

Mastenbroek, C., G. Burgers, and P. A. E. M. Janssen, The dynamical coupling of a wave model and a storm surge model through the atmospheric boundary layer, J. Phys. Oceanogr., 23, 1856-1866, 1993.

Miles, J., On the generation of surface waves by shear flows, J. Fluid Mech., 3, 185-204,

1957.

Monaldo, F. M., and D. R. Lyzenga, Comparison of Shuttle Imaging Radar-B ocean wave spectra with linear model predictions based on aircraft measurements, J. Geophys. Res., 93, 374-388, 1988.

Munk, W. H., and F. E. Snodgrass, Measurements of southern swell at the Guadalupe Islands, Deep-Sea Res., 4, 272-286, 1957.

Phillips, O. M., On the generation of waves by turbulent wind, J. Fluid Mech., 2, 417-445, 1957.

Plant, W. J., A relationship between wind stress and wave slope, J. Geophys. Res., 87, 1961-1967, 1982.

Plant, W. J., Reconciliation of theories of synthetic aperture radar imagery of ocean waves, J. Geophys. Res., 97, 7493-7501, 1992.

Plant, W. J. and W. C. Keller, The two-scale radar wave probe and SAR imagery of the ocean, J. Geophys. Res., 88, 9776-9784, 1983.

Plant, W. J. and W. Alpers, An introduction to SAXON-FPN, J. Geophys. Res., 99, 9699-9703, 1994.

Raney, R. K., and P. W. Vachon, Synthetic aperture radar imaging of ocean waves from an airborne platform: focus and tracking issues, J. Geophys. Res., 93, 12475-12486, 1988.

Raney, R. K., P. W. Vachon, R. A De Abreu, and A. S. Bhogal, Airborne SAR obersvations of ocean surface waves penetrating floating ice, IEEE Trans. Geosci. Remote Sensing, 27, 492-500, 1989.

Rosenthal, W., F. Ziemer, R.K. Raney, and P. Vachon, Removal of 180° ambiguity in SAR images of ocean waves, In Proc. IGARSS'89, IEEE Press, Piscataway, NJ, 1989.

Schulz-Stellenfleth, J., and S. Lehner, A new SAR inversion scheme for ocean waves traveling into sea ice, In Proc. IGARSS'99, IEEE Press, Piscataway, NJ, 1999.

Schulz-Stellenfleth, J., S. Lehner, and K. Hasselmann, ERS SAR observations of ocean waves traveling into sea ice, J. Geophys. Res., submitted, 1999.

Scoon, A., I. S. Robinson, and P. J. Meadows, Demonstration of an improved calibration scheme for ERS-1 SAR imagery using a scatterometer wind model, Int. J. Remote Sensing, 12, 413-418, 1996.

Snodgrass, F. E., G. W. Groves, K. Hasselmann, G. R. Miller, W. H. Munk and W. H. Powers, Propagation of ocean swell across the Pacific, Phil. Trans. Roy. Soc. Lond.

A, 249, 431-497, 1966.

- Sverdrup, H. U., and W. H. Munk, Wind, sea, and swell: Theory of relations for forecasting, Scripps Institution of Oceanography New Series, No. 303 H.O. Pub. No. 601/Technical Report No. 1, U.S. Navy, U.S. Hydrographic Office Publication, La Jolla, California, 1947.
- SWAMP Group, Ocean Wave Modeling, Plenum Press, New York, 256 pp, 1985.
- Swift, C. F., and L. R. Wilson, Synthetic aperture radar imaging of moving ocean waves, *IEEE Trans. Antennas Propag.*, 27, 725–729, 1979.
- Tucker, M. J., The imaging of waves by satellite synthetic aperture radar: the effect of surface motion, *Int. J. Remote Sensing*, *6*, 1059–1074, 1985.
- Ulaby, F. T., R. K. Moore, and A. K. Fung, *Microwave Remote Sensing*, Artech House, Dedham, Massachusetts, 3 Vol., 1986.
- Vachon, P. W., and R. K. Raney, Resolution of the ocean wave propagation direction in SAR imagery, *IEEE Trans. Geosci. Remote Sensing*, 29, 105–112, 1991.
- Vachon, P. W., and J. C. West, Spectral estimation techniques for multilook SAR images of ocean waves, *IEEE Trans. Geosci. Remote Sensing*, 30, 568–577, 1991.
- Vachon, P. W. and F. W. Dobson, Validation of wind vector retrieval from ERS-1 SAR images over the ocean, *Global Atmos. Ocean Sys.*, 5, 177–187, 1996.
- Vachon, P. W., J. W. M. Campbell, and F. W. Dobson, Comparison of ERS and RADAR-SAT SAR's for wind and wave measurements, In Proc. of the Third ERS Symposium, ESA SP-414, Vol. 3, ESA Publications Division, ESTEC, Noordwijk (NL), 1997a.
- Vachon, P. W., J. W. M. Campbell, and F. W. Dobson, ERS and RADARSAT SAR images for wind and wave measurement, In Proc. of CEOS Wind and Wave Validation Workshop, ESTEC, ESA WPP-147, ESA Publications Division, Noordwijk (NL), 57–60, 1997b.
- Valenzuela, G. R., Theories for the interaction of electromagnetic and ocean waves: A review, *Bound. Layer Meteorol.*, 13, 61–85, 1978.
- Valenzuela, G. R., An asymptotic formulation for SAR images of the dynamical ocean surface, *Radio Sci.*, 15, 105–114, 1980.
- WAMDI Group, The WAM model—a third generation ocean wave prediction model, J. Phys. Oceanogr., 18, 1775–1810, 1988.
- WASA Group, Changing waves and storms in the Northeast Atlantic?, Bull. Amer. Meteorol. Soc., 79, 741–760, 1998.
- Weber, S. L., H. von Storch, P. Viterbo, and L. Zambresky, Coupling an ocean wave model to an atmospheric general circulation model, *Climate Dyn.*, 9, 63–69, 1993.
- Weisse, R., and E. F. Alvarez, The European Coupled Atmosphere Wave Ocean Model: ECAWOM, MPI-Report No. 116, Max-Planck-Institut Meteorologie, Hamburg, 1997.
- Wilde, A., C. Brüning, W. Alpers, V. Etkin, K. Litovchenko, A. Ivanov, and V. Zajtsev, Comparison of ocean wave imaging by ERS-1 and ALMAZ-1 synthetic aperture radar, In Proc. of the Second ERS-1 Symposium, ESA SP-361, ESA Publications Division, ESTEC, Noordwijk (NL), 239–245, 1994.
- Wright, J. W., A new model for sea clutter, *IEEE Trans. Antennas Propag.*, 16, 217–223, 1968.
- Zurk, L. M. and W. J. Plant, Comparison of actual and simulated synthetic aperture radar image spectra of ocean waves, *J. Geophys. Res.*, 101, 8913–8931, 1996.

Patrick Heimbach, Department of Earth and Planetary Sciences, Room 54-1518, Massachusetts Institute of Technology, 77 Massachusetts Avenue, Cambridge, MA 02139, U.S.A. (email, heimbach@mit.edu; fax, +1-617-253-4464)